Three-dimensional analysis of the screening effectiveness of hollow pile barriers for foundation-induced vertical vibration

Pei-hsun Tsai [a], Zheng-yi Feng [b,*], Tin-lon Jen [a]

[a] *Department of Construction Engineering, Chaoyang University of Technology, Taichung 413, Taiwan*
[b] *Department of Soil and Water Conservation, National Chung Hsing University, Taichung 402, Taiwan*

Abstract

The study applies the three-dimensional boundary element method in frequency domain to investigate the screening effectiveness of circular piles in a row for a massless square foundation subject to harmonic vertical loading. Four types of piles were studied: steel pipe piles, concrete hollow piles, concrete solid piles and timber piles. A parametric study was undertaken to examine the effects of pile dimensions, operational frequency, and source distance on the screening effectiveness. The results showed that screening effectiveness of steel pipe piles is generally better than that of solid piles, and that a concrete hollow pile barrier can be ineffective due to its stiffness. The influence of pile length on screening effectiveness is more significant than that of pile spacing and the distance between the vibrating foundation and the pile barrier.
© 2007 Elsevier Ltd. All rights reserved.

1. Introduction

If the vibration level of construction, traffic or machine operation is too high, environmental quality will be degraded and distress people. Often it may cause cost overruns due to bad production rates of high-tech plants which have strict limitation on vibration. Therefore, reduction or isolation of vibration for required areas is an important issue. Among the various isolation methods, installation of barriers between a vibration source and the area of protection is deemed one of the best solutions. Trenches are often used for barriers; however, there are limitations such as constructible depth and stability of the trench. Piles, therefore, are studied for vibration barriers.

2. Review of previous analyses

In an experimental approach, Barkan [1] used sheet piles and open trenches to isolate and protect a building from traffic vibration, but at that time the screening effectiveness for the trench was not well known. McNeill et al. [2] described some successful applications of vibration isolation with open trench and sheet piles. Woods [3] presented field experimental results using open trenches for wave isolation. He defined the amplitude reduction ratio and showed the amplitude reduction ratio contour diagrams for ground surface displacement amplitude reduction ratio near the trench. He considered the amplitude reduction ratio should be smaller or equal to 0.25 for a good isolation mechanism. Woods et al. [4] used the principle of holography to simulate vibration in half-space to observe passive screening effectiveness of hollow cylindrical piles as barriers. They concluded that the diameter of the piles should be greater than 0.6 times of Rayleigh wave (R-wave) length, L_R, and the net spacing between the piles should be smaller than $0.4L_R$. Liao and Sangrey [5] studied the

---
* Corresponding author. Tel.: +886 4 22840381x222; fax: +886 4 22876851.
E-mail address: tonyfeng@dragon.nchu.edu.tw (Z.Y. Feng).

propagation of sound waves in fluid media using model piles as passive vibration reduction barriers. They found that the screening effectiveness of soft pile is better than hard pile (e.g. concrete pile). For a hollow pile barrier to have better screening effectiveness, the hollow piles must be small in diameter and made with elastic materials. The screening effectiveness of a double row pile barrier is better than a single row pile barrier. However, if the spacing of piles in a single row barrier is small enough, the screening effectiveness of a single row pile barrier can be better than that of a double row pile barrier. The upper limit of the pile spacing is $0.4L_R$ for an effective vibration reduction. Haupt [6] performed model tests for analyses of vibration reduction. He used an open trench, a concrete in-filled trench, and hollow piles in a row as the vibration reduction mechanisms. His research showed that efficiency of vibration reduction is related to the cross-sectional area of the trench. The efficiency increases with increasing depth of the trench.

For numerical approaches, Wass [7] used the finite element method (FEM) to study the influence of trenches on horizontal shear waves (SH-wave). His results showed the vibration reduction efficiency of open trenches is not good at high frequencies, and only good at some low frequencies. Aboudi [8] installed barriers in elastic half-space and used finite difference method (FDM) to calculate the ground surface response. He concluded that the behavior of Rayleigh wave propagation will be influenced by barriers. Haupt [9] performed experiments to verify his finite element analysis on the vibration reduction subject. He found complex wave propagation near the barriers. For stiffer in-filled materials, the efficiency of vibration reduction relates to the cross-sectional area of the trench; and for softer in-filled materials, the efficiency relates to the shape of the trench. Segol et al. [10] applied FEM to discuss 2-D vibration reduction for open and in-filled trenches in layered stratum. Fuyuki and Matsumoto [11] adopted FDM to investigate Rayleigh waves when they reach an open trench. May and Bolt [12] employed FEM to examine the isolation effects of open trenches on SH-wave in two layer soil systems. They found that when vibration frequencies are between 4 Hz and 6 Hz, and the depth of a trench is greater than $0.6L_R$, the power spectral ratio of SH-waves can be reduced to only 6% of free field (i.e. no trench). However, when operational frequency is smaller than 4 Hz, the power spectral ratio could be enlarged to over 200%. Avilles and Sanchez-Sesma [13] inspected the vibration reduction effect of 8 solid piles on compression wave (P-wave), SH-wave, vertical shear wave (SV-wave). From the results, it showed that among these three waves, the efficiency of vibration reduction of solid piles to SV-wave is better, but worse for P-wave. A pile diameter between 1/4 and 1 times of shear wave length is most efficient. Net spacing of piles is found most important to the influence of dimension and arrangement of piles. Emad and Manolis [14] utilized the boundary element method (BEM) with constant elements to research the efficiency of vibration

reduction of rectangular and circular open trench. Screening effectiveness using vibration amplitude as indicator was evaluated for some particular locations. Beskos et al. [15] employed BEM with constant element to discuss the influence on vibration reduction using open and in-filled trenches. He concluded the efficiency of vibration reduction of open trenches is better than that for in-filled trenches. Dasgupta et al. [16,17] applied 3-D frequency domain BEM with full domain fundamental solution to analyze rigid surface foundation subjected to harmonic loading and discussed vibration reduction of open and in-filled trenches. Avilles and Sanchez-Sesma [18] developed theoretical models to study the distribution of amplitude reduction behind circular solid piles in a row when subjected to SV-wave and R-wave. They found when the diameter of a pile equals to $0.25L_R$, and the pile length equals to $2 L_R$, the screening effectiveness can be optimized. Ahmad and Al-Hussaini [19] utilized 2-D BEM to research the efficiency of vibration reduction for open and in-filled trench under horizontal or vertical vibration mode. A simplified design method was proposed using the influence parameters, including frequency, location of trench, wave velocity, properties of in-filled material, Poisson's ratio, and damping ratio. Klein et al. [20] showed that depth of trench is a critical parameter in screening effectiveness. Kattis et al. [21,22] also used 3-D frequency domain BEM to calculate the screening effectiveness of piles in a row for the same assumption. The piles were assumed as tubular or solid and have circular and square cross-sections. Their tubular piles are only treated as long cylindrical cavities for simplicity. They showed that the shape of the pile does not much influence screening effectiveness. They concluded that net spacing of piles is the major influencing factor: the smaller the net spacing, the better the screening effectiveness of a barrier.

3. Overview of study

From the above review, researches for vibration reduction mainly focused on open-trench and in-filled trench. They are limited to circular cavities or square cavities in a row or solid pile. Analysis using structured hollow/pipe piles is rare. Therefore, this paper focuses on the efficiency of structured hollow piles (not just using cavities as piles). The materials for the hollow piles are concrete or steel. In addition, concrete solid piles and timber solid pile were also analyzed for comparisons. Rigid massless square foundations subjected to vertical harmonic loading were modeled. The barriers are arranged using 8 piles in a row. Numerical analyses were performed using 3-D BEM to calculate vertical vibration amplitudes behind a pile barrier and amplitude reduction ratio. There are four pile types studied, including steel pipe pile, concrete hollow pile, concrete solid pile, and timber solid pile.

Woods [3] proposed an averaged amplitude reduction ratio, $\overline{A_{ry}}$, for evaluation of screening effectiveness. The amplitude reduction ratio, A_{ry}, is first computed using

Eq. (1), which is the ratio between amplitude with piles and amplitude without piles.

$$A_{ry} = \frac{\text{Amplitude with the pile barrier}}{\text{Amplitude without pile barrier}} \tag{1}$$

To evaluate the screening effectiveness of piles, the averaged amplitude reduction ratio, $\overline{A_{ry}}$, is calculated using the rectangular area, A, right behind the piles. The area is defined as the area of one Rayleigh wave length long multiples the width of the piles in a row. The amplitude reduction ratio, A_{ry}, is averaged becoming $\overline{A_{ry}}$ as shown in Eq. (2):

$$\overline{A_{ry}} = \frac{1}{A} \int A_{ry} \, dA \tag{2}$$

In this study, parametric studies were performed by varying dimension and arrangement of piles, including net spacing between piles in a row, pile length, the source distance from the central pile of the barrier to the center of vibration foundation, and operational frequency. The results can be useful in pile barrier design to achieve vibration reduction, and beneficial to plan experimental work. If the number of the piles in the design is greater or less than eight, additional analyses can be performed using the numerical scheme introduced in this study.

4. Boundary element method

The time domain equation of motion for a homogeneous, isotropic, and linear elastic body can be expressed as:

$$\sigma_{ij,j}(x,t) + \rho f_i(x,t) = \rho \ddot{u}_i(x,t) \quad i,j = x,y,z \tag{3}$$

where $\ddot{u}_i(x,t)$ is the acceleration; $\sigma_{ij}(x,t)$ is the stress; ρ and $f_i(x,t)$ are mass density and body force per unit mass, respectively. The u_i and f_i are complex variables.

Using the Fourier transform of Eq. (3), the governing equation of motion in frequency domain takes the form:

$$\sigma_{ij,j}(x,\omega) + \rho f_i(x,\omega) = -\rho \omega^2 u_i(x,\omega) \tag{4}$$

where ω is the Fourier transform parameter and is equal to the excitation frequency in this study.

The fundamental solution, $U_{ij}(\mathbf{x},\mathbf{y},\omega)$, is defined as the displacement field at field point x in i direction due to the concentrated force with a unit amplitude acting in the j direction at loading point y. The fundamental solution of traction field is expressed as $T_{ij}(\mathbf{x},\mathbf{y},\omega)$. The 3-D fundamental solution, $U_{ij}(\mathbf{x},\mathbf{y},\omega)$, of steady state elastodynamic in infinite medium domain, satisfies the following equation:

$$\sigma_{ij,j}(x,y,\omega) + \rho \omega^2 u_i(x,y,\omega) = -\delta_{ij}\delta(y,x) \tag{5}$$

The solution of Eq. (5) was obtained as Eq. (6) [23].

$$U_{ij} = \frac{1}{4\pi\mu}\left[L(k_T)\delta_{ij} + \frac{1}{k_T}M_{,ij} \right] \tag{6}$$

where

$$L(k_T) = \frac{e^{ik_T r}}{r}, \quad M = L(k_T) - L(k_L)$$

$M_{,ij} = \frac{\partial^2 M}{\partial X_i \partial X_j}$, $r = |x - y|$, X_i is the three directional (x,y,z) components of the vector from loading point y to field point x.

δ_{ij} = the Kronecker delta, $\delta_{ij} = 1$, when $i = j$; $\delta_{ij} = 0$, when $i \neq j$.
c_T = shear wave velocity,
c_L = dilational wave velocity,
k_T = wave numbers of shear wave,
k_L = wave numbers of dilational wave.

The fundamental solution of traction field is calculated from the fundamental solution U_{ij} as:

$$T_{ij}(\mathbf{x},\mathbf{y},\omega) = D_{ijk}(\mathbf{x},\mathbf{y},\omega)n_k \tag{7}$$

where n_k is the unit outward normal vector at field point x;

$$D_{ijk} = \lambda U_{il,l}\delta_{jk} + \mu(U_{ij,k} + U_{ik,j}) \tag{8}$$

where λ, μ are Lamé's elastic constants.

In these expressions of U_{ij} and T_{ij} contains the terms of order $(kr)^{-2}r^{-1}$ and $(kr)^{-2}r^{-2}$, respectively, and k stand for either k_T or k_L. Therefore, if r is near to zero or low frequency range, i.e., $kr \to 0$, the integrals of fundamental solution become singular. Kitahara et al. [24] suggested two types of expressions of fundamental solution. Regular type is used for all case except $kr \to 0$ and singular type is used for $kr \to 0$.

1. Regular type [24]

$$U_{ij} = \frac{k_T}{4\pi\mu}[(\text{AU1})\delta_{ij} - (\text{AU2})r_{,i}r_{,j}] \tag{9}$$

$$\begin{aligned}T_{ij} &= -[\lambda\delta_{jk}U_{im,m} + \mu(U_{ij,k} + U_{ik,j})]n_k \\ &= \frac{k_T^2}{4\pi}\Big[\{((\text{AT2}) - (\text{AT1}))\delta_{ij} + 2((\text{AT3}) - 2(\text{AT2}))r_{,i}r_{,j}\}r_{,k}n_k \\ &\quad + \Big\{\frac{\lambda}{\mu}((\text{AT3}) - (\text{AT1})) + 2\Big(\frac{\lambda}{\mu}+1\Big)(\text{AT2})\Big\}r_{,i}n_j + ((\text{AT2}) - (\text{AT1}))r_{,j}n_i \Big] \end{aligned} \tag{10}$$

The detail formulation for AU1, AU2, AT1, AT2, and AT3 can be found in Kitahara et al. [24].

2. Singular type [24]

$$U_{ij} = \hat{U}_{ij} + \overline{U}_{ij} \tag{11}$$

$$T_{ij} = \hat{T}_{ij} + \overline{T}_{ij} \tag{12}$$

where

$$\hat{U}_{ij} = \frac{1}{16\pi\mu(1-v)r}[(3-4v)\delta_{ij} + r_{,i}r_{,j}] \tag{13}$$

$$\hat{T}_{ij} = \frac{1}{8\pi(1-v)r^2}[\{(1-2v)\delta_{ij} + 3r_{,i}r_{,j}\}r_{,k}n_k - (1-2v)(r_{,i}n_j - r_{,j}n_i)] \tag{14}$$

with v denoting Poisson's ratio. This $\hat{U}_{ij}$ coincides with the fundamental solution of the elastostatics. The term $\hat{U}_{ij}$ has

the singularity r^{-1}, and the term $\hat{T}_{ij}$ has the singularity r^{-2}. These singularities can be treated in elastostatics problem. This treatment makes $\overline{U}_{ij}$ and $\overline{T}_{ij}$ become regular when r is approaching zero as following:

$$\overline{U}_{ij} = \frac{1}{4\pi\mu}[\phi\delta_{ij}] - \psi r_{,i}r_{,j}] \tag{15}$$

$$\overline{T}_{ij} = \frac{1}{4\pi}\left[\left\{\left(\frac{\psi}{r} - \phi'\right)\delta_{ij} + 2\left(\psi' - \frac{2\psi}{r}\right)r_{,i}r_{,j}\right\}r_{,k}n_k \right.$$
$$\left. + \left\{\frac{\lambda}{\mu}(\psi' - \phi') + 2\left(\frac{\lambda}{\mu} + 1\right)\frac{\psi}{r}\right\}r_{,i}n_j + \left(\frac{\psi}{r} - \phi'\right)r_{,j}n_i\right] \tag{16}$$

The ϕ and ψ in Eqs. (15) and (16) are:

$$\phi = \sum_{n=1}^{\infty}\frac{(ik_T)^n}{n!}r^{n-1} + \frac{1}{k_T^2}\sum_{n=3}^{\infty}a_n(n-1)r^{n-3} \tag{17}$$

$$\psi = -\frac{1}{k_T^2}\sum_{n=4}^{\infty}a_n(n-1)(n-3)r^{n-3} \tag{18}$$

where $a_n = i^n\frac{(k_T^n - k_L^n)}{n!}$, $\phi' = \frac{\partial\phi}{\partial r}$, and $\psi' = \frac{\partial\psi}{\partial r}$.

By applying Betti's reciprocal theorem [25], Eq. (4) can be transformed into Eq. (19) as:

$$\int_S [t_i(\mathbf{x},\omega)U_{ij}(\mathbf{x},\mathbf{y},\omega) - T_{ij}(\mathbf{x},\mathbf{y},\omega)u_i(\mathbf{x},\omega)]\,d\Gamma$$
$$= u_j(\mathbf{y},\omega), \quad \mathbf{y} \in \mathbf{V} \tag{19}$$

Traction, t_i, is complex variable. We assume that no wave can be reflected from infinite, i.e., field quantities at infinite must satisfy Sommerfeld's radiation condition [24]. Therefore, Eq. (19) can then be expressed as:

$$\int_{\partial S} [t_i(\mathbf{x},\omega)U_{ij}(\mathbf{x},\mathbf{y},\omega) - T_{ij}(\mathbf{x},\mathbf{y},\omega)u_i(\mathbf{x},\omega)]\,d\Gamma = u_j(\mathbf{y},\omega) \tag{20}$$

where ∂S is ground surface and pile surface boundary, and $\mathbf{y} \in \mathbf{V}$. If $\mathbf{y}$ is belongs to boundary ∂S, the boundary integral equation is then established as:

$$\int_{\partial S} [t_i(\mathbf{x},\omega)U_{ij}(\mathbf{x},\mathbf{y},\omega) - T_{ij}(\mathbf{x},\mathbf{y},\omega)u_i(\mathbf{x},\omega)]\,d\Gamma = C_{ij}u_i(\mathbf{y},\omega) \tag{21}$$

Eq. (21) is the governing boundary integral equation. C_{ij} can be computed by the Cauchy principal value [26]. If boundary ∂S is smooth in the neighborhood of $\mathbf{y}$, C_{ij} can be computed as:

$$C_{ij} = \frac{1}{2}\delta_{ij} \tag{22}$$

The boundary ∂S can be discretized into n constant element boundary with constant stress and displacement vectors on the boundary. Eq. (21) can be expressed as a matrix equation:

$$C_{ij}u_i + \sum_{j=1}^{n}\widetilde{H}_{ij}u_j = \sum_{j=1}^{n}G_{ij}t_j \tag{23}$$

where

$$C_{ij} = \frac{1}{2}\delta_{ij} \tag{24}$$

$$\widetilde{H}_{ij} = \int_{\Gamma_j} T_{ij}(x,y,\omega)\,d\Gamma_j \tag{25}$$

$$G_{ij} = \int_{\Gamma_j} U_{ij}(x,y,\omega)\,d\Gamma_j \tag{26}$$

Therefore, Eq. (23) can be simplified to:

$$\sum_{j=1}^{n}H_{ij}u_j = \sum_{j=1}^{n}G_{ij}t_j \tag{27}$$

where

$$H = C + \widetilde{H} \tag{28}$$

Eq. (27) can be put in the following matrix form:

$$[H] \cdot \{U\} = [G] \cdot \{T\} \tag{29}$$

By substituting the boundary condition into Eq. (29), the following governing equation can be obtained.

$$[A] \cdot \{X\} = \{F\} \tag{30}$$

Using the correspondence principle [27], material damping of soil can be taken into account by replacing the wave velocity in complex form; i.e.,

$$c_L^* = c_L\sqrt{1 - 2i\beta}, \quad c_T^* = c_T\sqrt{1 - 2i\beta} \tag{31}$$

where β is the material damping ratio, the symbol $*$ denotes complex form. The unknown vector $\{X\}$ in Eq. (30) can be solved by the Gaussian elimination method. The displacement and traction of all boundary elements can be obtained subsequently.

5. Numerical model

This study assumes the soil and foundation form a perfectly bonded contact: the foundation remains in place on the ground while vibrating, and the displacement of soil is the same as the displacement of the foundation. To make sure the foundation is rigid; all elements at the foundation should be all assigned the same vertical displacement amplitude. For those elements at ground surface, zero traction is assumed (traction free). Meanwhile, for the elements of pile heads and those on the surface inside the hollow piles, the traction is also zero. In this study, there is no need to use interface elements between piles and soils because the difference in displacement between piles and soils is very small. Therefore, the piles and soils are assumed to be perfectly bonded, i.e., soil and pile have their individual elements on the interfaces. The displacements of soil elements on the interfaces are equal to those of pile elements in the other side of the interfaces. The tractions of soil elements and pile elements are in the same magnitude but acting in opposite directions on the interfaces. However, numbers of elements on the interfaces between piles and soil are counted twice.
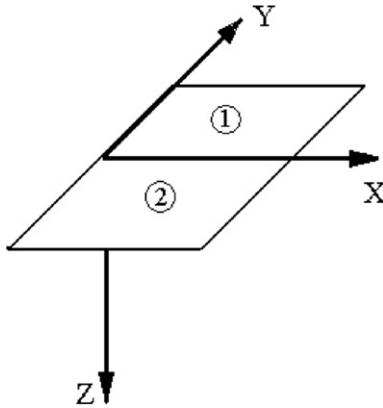
Fig. 1. The symmetrical model domain in this study (symmetry in xz-plane).

In numerical analysis, if a physical problem presents symmetry, taking advantage of it results in less computation time and computer memory. In this study, there is a symmetrical plan located at the vertical plan cutting through the center of the foundation and center of the row of piles. The boundary conditions at the plan are that the normal displacement components of the plan are zero, and the tangential traction components of the plan are zero.

In this study, the model domain is designed to be symmetrical in xz-plane, thus the degrees of freedom (unknowns) can be significantly reduced. Only a half of the domain is discretized as shown in Fig. 1 and the deriva-tions of the boundary element system equations are explained as following.

Because of symmetry in xz-plane, the displacement field has the relationships:

$$u_{1x} = u_{2x}, \quad u_{1y} = -u_{2y}, \quad u_{1z} = u_{2z} \tag{32}$$

where the subscript 1 and 2 stand for Zone 1 and Zone 2 in Fig. 1. A typical boundary element mesh for the study applying symmetries is shown in Fig. 2.

The boundary element system equations can be expanded as:

$$\sum H_{1x1x}u_{1x} + H_{1x1y}u_{1y} + H_{1x1z}u_{1z} + H_{1x2x}u_{2x}$$
$$+ H_{1x2y}u_{2y} + H_{1x2z}u_{2z} = \sum G_{ij}t_j \tag{33}$$

Due to symmetry, u_{2x}, u_{2y} and u_{2z} can be replaced by u_{1x}, u_{1y} and u_{1z}, respectively. Therefore, Eq. (33) can be re-writ-ten as:

$$\sum((H_{1x1x} + H_{1x2x})u_{1x} + (H_{1x1y} - DH_{1x2y})u_{1y}$$
$$+ (H_{1x1z} + H_{1x2z})u_{1z}) = \sum G_{ij}t_j \tag{34}$$

Traction field can be treated in the similar approach. Therefore, the total degrees of freedom of the boundary element model can be reduced to one-half of the original one.

Constant boundary elements are adopted. The numeri-cal program used in this study is coded according to the above 3-D boundary element theory using FORTRAN language. The number of element in a mesh is often
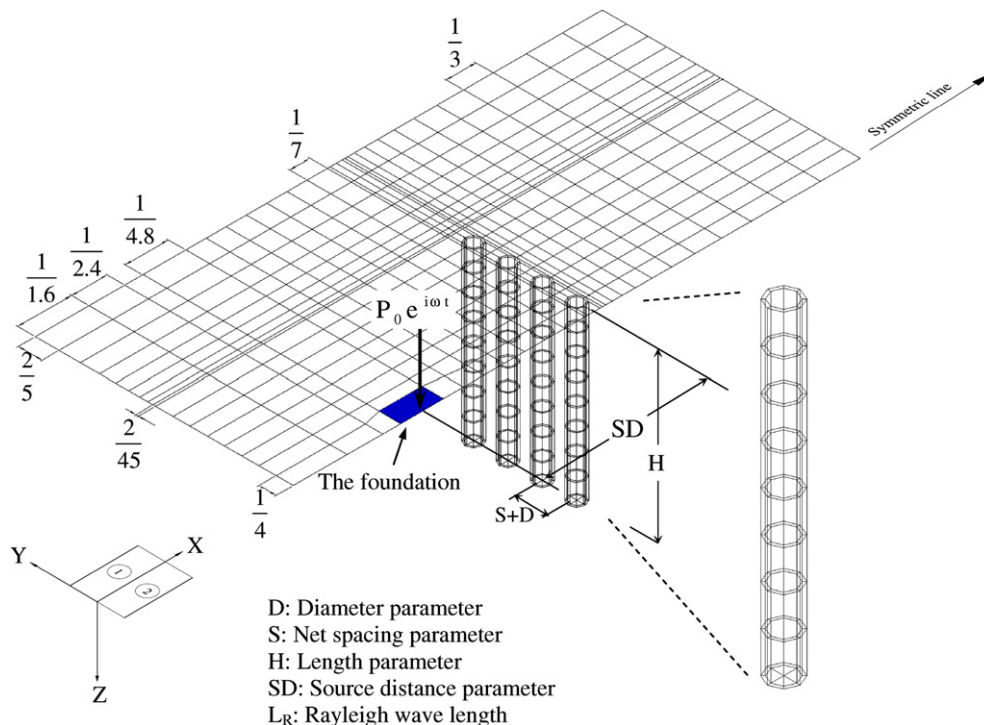

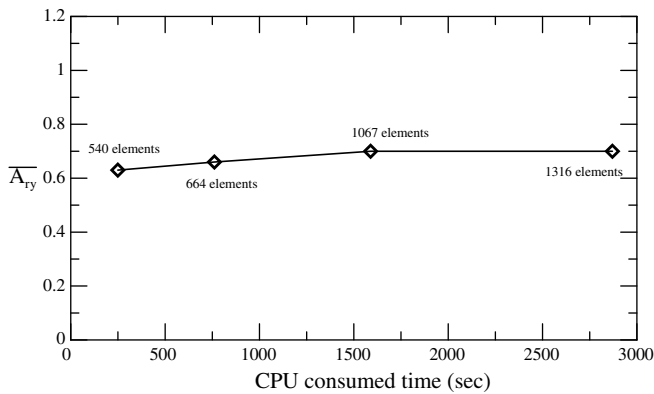Fig. 2. A typical boundary element mesh for the study.

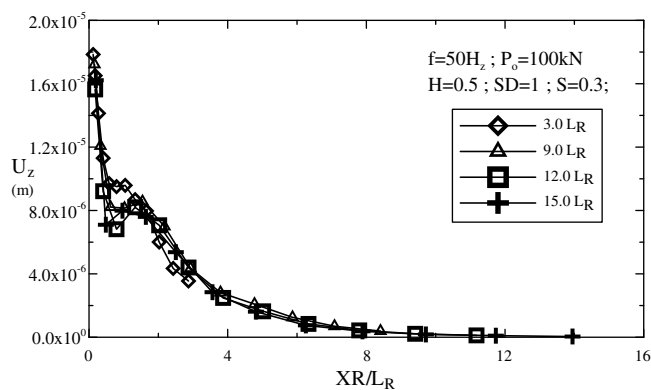Fig. 3. The $\overline{A_{ry}}$ and CPU consumed time.

Fig. 4. Results of mesh study for decision of the boundary behind a concrete solid pile barrier.

constricted to RAM size and CPU. To decide an optimum mesh, the authors selected 4 element meshes with 540, 664, 1067, and 1316 elements to compare precision of results. The comparison is shown in Fig. 3 and the numerical difference becoming approximately "steady". There is about 5.7% numerical difference between using 1067 and 1316 elements. Therefore, by considering the CPU consumed time and numerical difference, the mesh of 1067 elements (747 for soil and 320 for pile) was selected for solid pile barriers.

For hollow pile barriers, a typical mesh of 1355 (779 for soil and 576 for pile) was selected as shown in Fig. 2 for symmetrical half domain. There are three displacement directions of each element; therefore, there are totally 4065 degrees of freedom in the numerical system. We used a high-performance computer (IBM SP SMP, 4CPU×42-node, 184 GB RAM) for the computations.

In Eqs. (25) and (26), the integration of U_{ij} and T_{ij} were calculated by standard numerical integration method, using the values of U_{ij} and T_{ij} at the Gaussian integration points multiple the "weights". The Gaussian integration points and "weights" can be referred in Brebbia [28]. The geometry of each boundary elements will be mapped in to a "master element" for numerical Gaussian integration as stated in Becker et al. [29].

To investigate the screening effectiveness of pile barriers and the influencing factors, Rayleigh wave length, L_R, was used to normalize the pile dimensions. As shown in Fig. 2, the pile length, h, is divided by L_R to be the pile length parameter, H. The net spacing between piles, s, is divided by L_R to be the net spacing parameter, S. The source distance, sd, is normalized to be the source distance parameter, SD. In addition, the pile diameter, d, and hollow pile thickness, t, to be D and T, respectively.

For the ground surface right behind the pile barrier, the elements were discretized into finer rectangle elements, the size of element between $L_R/25$ and $L_R/5$, because these are the major areas for evaluating screening effectiveness. Generally, element size is larger for those elements away from the barrier.

To decide the extent of the mesh boundary behind a barrier for numerical analyses, a mesh study was performed using $3L_R$, $9L_R$, $12L_R$, and $15L_R$ as the mesh boundary for concrete solid pile barriers. A harmonic force, $P_0 = 100$ kN with vibration frequency $f = 50$ Hz and $L_R = 5$ m, was assumed acting on the foundation. The geometry parameters of the solid piles are: $H = 0.5$, $S = 0.3$, SD = 1, $D = 0.2$. Vertical amplitudes of ground surface were calculated as shown in Fig. 4. It is found that the amplitudes for the above four boundary extensions are very similar. Therefore, using $3L_R$ distance for the mesh boundary behind the barrier should be accurate enough and was adopted for the subsequent numerical analyses.

To verify the BEM code developed in this research, a numerical analysis on vibration reduction ratio of a concrete solid pile barrier was compared with the results from Kattis et al. [21]. The geometry parameters of the solid pile barrier are: $H = 1.0$, $S = 0.1$, SD = 1.5, $D = 0.2$. The assumed material properties of soil and concrete are listed in Table 1. The frequency of vibration foundation is $f = 50$ Hz. The size of the foundation is 0.8 m × 0.8 m. The vibration reduction ratio at each element is presented in Fig. 5. It can be observed that the amplitude reduction ratio is much smaller right behind the pile barriers. By graphically comparison, results in Fig. 5 is close to that of Kattis et al. [21] for the identical solid pile barrier conditions. For further comparison, a numerical analysis was performed for cylindrical cavity barrier by assigning soil properties to hollow piles. The results shows that the average amplitude reduction ratio, $\overline{A_{ry}}$, of 8 cylindrical cavities is 0.838, while results of Kattis is 0.812. There is only 3%

Table 1
Material properties of soil and piles in this study

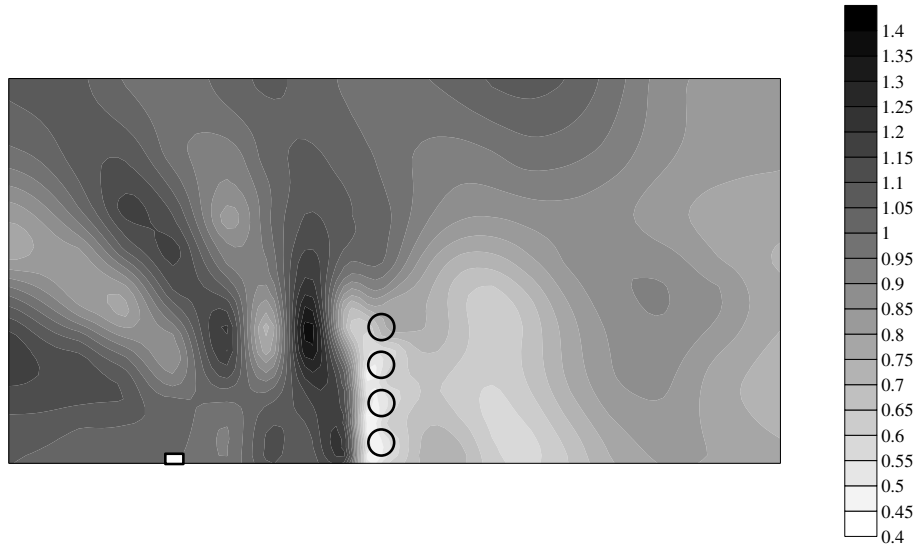|	Soil	Steel pipe [30]	Concrete	Timber [31]
Shear modulus G, MN/m²	132	79,300	4526.28	5580
Poisson's ratio v	0.25	0.3	0.25	0.29
Unit weight γ, kN/m³	17.5	75	23.5	4.2
Material damping ratio, β	0.05	0.03	0.05	0.08

Fig. 5. Amplitude reduction ratios near the concrete solid pile barrier.

difference. Therefore, the accuracy of the developed BEM code for screening effectiveness of pile barriers system is validated.

6. Parametrical study for screening effectiveness

The vibration reduction effect will be different when different materials and types of piles are used. Four different types of piles including timber and concrete solid piles, and concrete and steel hollow piles were investigated for screening effectiveness for various pile dimension parameters and layouts, such as H, S and SD. The results were shown using the averaged vertical amplitude reduction ratio, $\overline{A_{ry}}$ as shown in Eq. (2). The elastic properties of the soil and piles are also listed in Table 1. The geometry parameters are listed in Table 2. The vibration frequency (f) of the foundation is assumed as 50 Hz. The velocity of Rayleigh waves in soil, v_R, is assumed as 250 m/s; thus, the wavelength of Rayleigh wave (L_R) is 5 m. The thicknesses parameter $T = t/L_R$, of the concrete hollow piles and steel pipe piles are both assumed to be 0.025; that is, the thickness of piles (t) = 12.5 cm for L_R = 5 m. The t = 12.5 cm is based on practical experience for concrete hollow piles. For comparison reason, the thickness of steel pipe piles is also justified as 12.5 cm. For the parameters listed in Table 2, a consid-

erable amount of results were generated. However, only partial and representative figures are selected to present in this paper.

For steel pipe pile, the isolation effectiveness generally increases with increasing pile length (Fig. 6). A pile with $H \geqq 1.5$ is capable of achieving an $\overline{A_{ry}} < 0.2$. For some cases, the $\overline{A_{ry}}$ slightly increased with increasing the length parameter H when H is greater than 1.5. This could be due to wave scattering or diffracting. However, the influence of this phenomenon is minor in design practice, because the difference is small. To investigate the influence of pipe pile's properties, the authors varied the shear modulus of pipe pile (G = 79,300 MN/m^2) for 0.33 G, 0.5 G, 2 G and 3 G, and density (γ = 75 kN/m^3) for 0.33γ, 0.5γ, 2γ and 3γ. Figs. 7 and 8 show the isolation effectiveness increases with increasing shear modulus and density of pipe pile, respectively. However, the influence of density is relatively smaller. As pipe pile's length is equal to a Rayleigh wave length (H = 1), the influence of shear modulus on isolation effectiveness is clear. The system is sensitive while H equals to one. In Fig. 9, it shows that influence of net spacing parameter, S, on screening effectiveness influence is insignificant. In Fig. 10, the $\overline{A_{ry}}$ increases and decreases slightly with increasing SD when H = 1; however, the variation is not obvious.

Table 2
Parameters for the numerical study

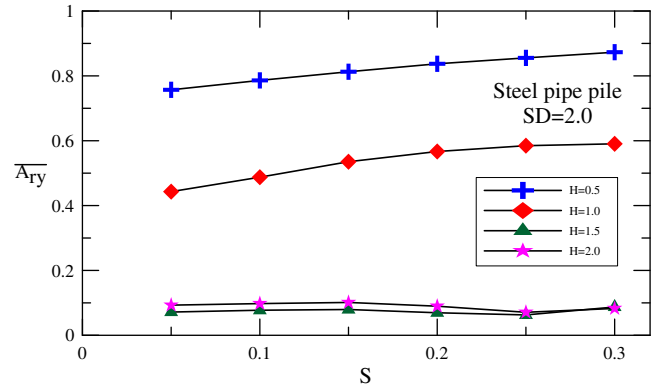| Purpose of analyses	Fixed parameters		Varying parameters	
Influence of pile length	D 0.2	S 0.05	H 0.5, 1.0, 1.5, 2.0	SD 1.0, 1.5, 2.0, 3.0
Influence of net spacing	D 0.2	SD 2.0	H 0.5, 1.0, 1.5, 2.0	S 0.05, 0.1, 0.15, 0.2, 0.25, 0.3
Influence of source distance	D 0.2	H 1.0	SD 1.0, 1.5, 2.0, 3.0	S 0.05, 0.1, 0.15, 0.2, 0.25, 0.3
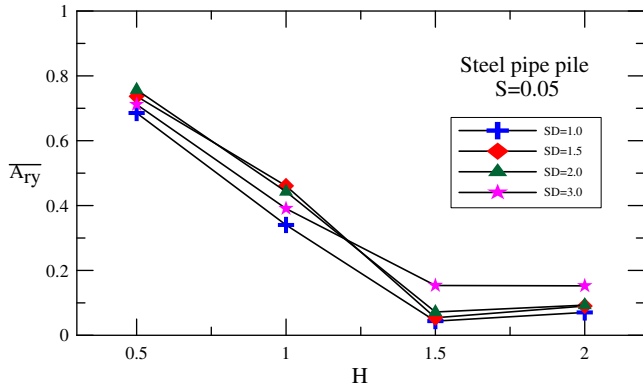
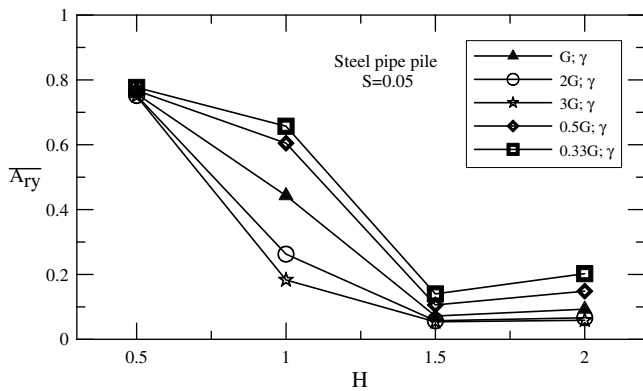Fig. 6. Influence of length parameter, H, on $\overline{A_{ry}}$-steel pipe pile.

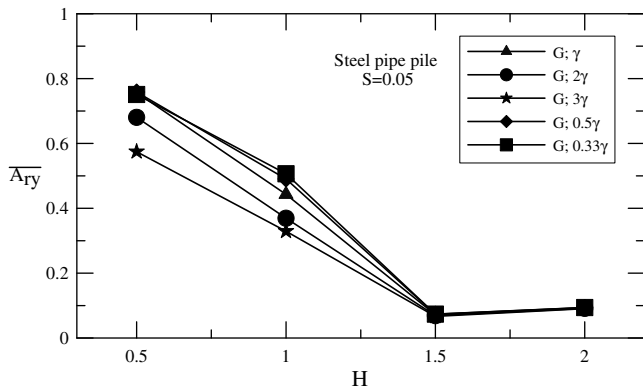Fig. 7. Influence of shear modulus of steel pipe pile on $\overline{A_{ry}}$.

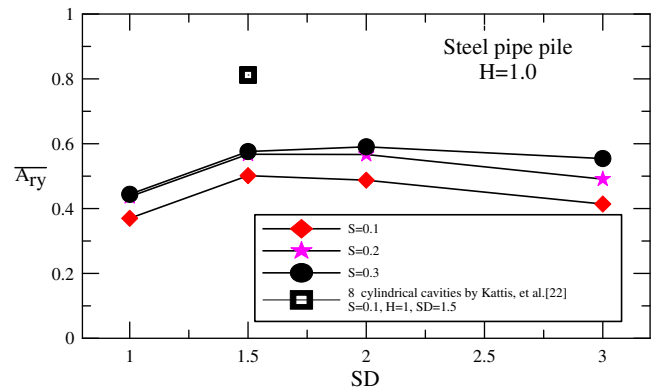Fig. 8. Influence of unit weight of steel pipe pile on $\overline{A_{ry}}$.

Fig. 9. Influence of net spacing parameter, S, on $\overline{A_{ry}}$-steel pipe pile.

Fig. 10. Influence of source distance parameter, SD, on $\overline{A_{ry}}$-steel pipe pile.

cylindrical cavity barrier can not be used to represent structured hollow pile barrier.

The screening effectiveness of concrete solid piles is also compared with the results of Kattis et al. [22] in Fig. 11. The numerical result of this study and that of Kattis et al. are very close. $\overline{A_{ry}}$ are 0.728 and 0.712, respectively.

For concrete hollow piles, the isolation effectiveness increases with increasing pile's length, but might not be so effective when $H > 1.5L_R$ (Fig. 12). It can be observed that the concrete hollow pile barriers in this study are inef-
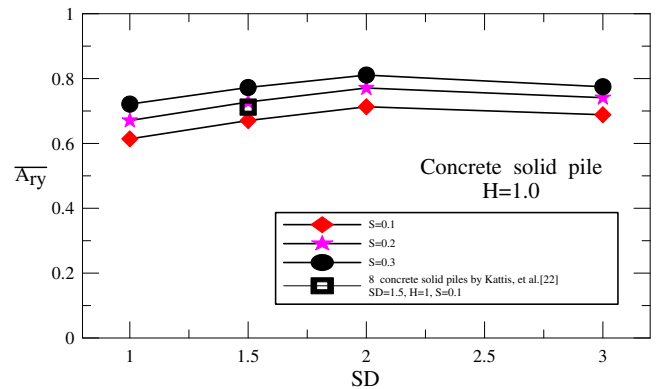

Fig. 11. Influence of source distance parameter, SD, on $\overline{A_{ry}}$-concrete solid pile.

The screening effectiveness results of steel pipe piles are compared with the results of Kattis et al. [22] which used 8 cylindrical cavities in Fig. 10. It is obvious that the wave propagation is quite different between cylindrical cavity barriers and steel pipe pile barriers. The discrepancy in $\overline{A_{ry}}$ is considerable. The $\overline{A_{ry}}$ of Kattis et al. [22] is 0.812, and $\overline{A_{ry}}$ of steel pipe pile barrier is 0.501. The result reveals that screening effectiveness between steel pipe pile barriers and cylindrical cavity pile barrier is very different; thus
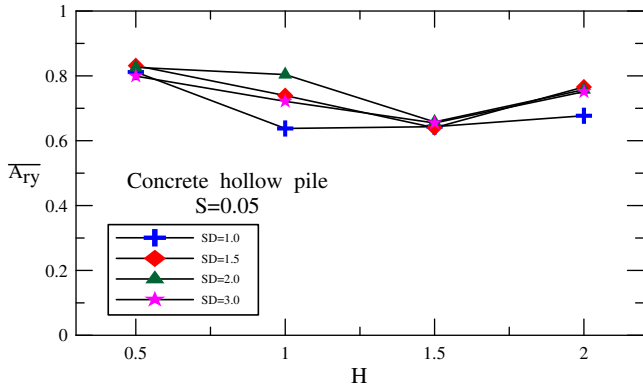
Fig. 12. Influence of length parameter, H, on $\overline{A_{ry}}$-concrete hollow pile.
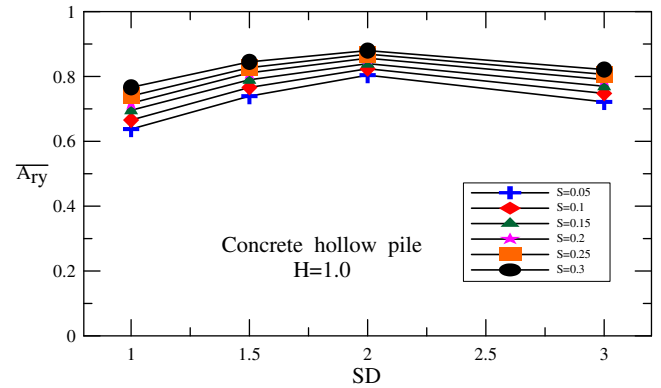

Fig. 14. Influence of source distance parameter, SD, on $\overline{A_{ry}}$-concrete hollow pile.

fective due to their $\overline{A_{ry}}$ are larger than 0.4. In Fig. 13, it shows that screening effectiveness is slightly better when S is small for concrete hollow piles. In Fig. 14, it shown the influence of source distance (SD) is not significant when the length parameter H equals to 1.0; and the trend of $\overline{A_{ry}}$ is similar to that of steel pipe pile (Fig. 10).

Generally, when the length parameter, H, increases, the values of $\overline{A_{ry}}$ becomes smaller (Fig. 15). However, when $H > 1.5$, $\overline{A_{ry}}$ slightly increases. Generally, for a smaller net spacing parameter (S), the $\overline{A_{ry}}$ is smaller for timber, concrete solid and hollow pile barriers (Fig. 16); but the trend is slightly reversed for steel pipe pile barriers. It could be that when $\overline{A_{ry}}$ is small and due to wave scattering/diffraction or computational error (about 3%), $\overline{A_{ry}}$ become sensitive for the steel pipe pile barriers. It is not easy to clearly identify its causes. However, in design practice, influence of this reversed trend is minor, because $\overline{A_{ry}}$ is already very small (effective). For the influence of SD shown in Fig. 17, the $\overline{A_{ry}}$ curves of the four types of piles are nearly flat, which means that the influence of SD on $\overline{A_{ry}}$ is not obvious.

From Figs. 15–17, we can observe that the screening effectiveness of steel pipe pile barriers is the best, while steel pipe pile has the largest shear modulus. The $\overline{A_{ry}}$ of concrete solid piles and timber piles are similar. This may be due to
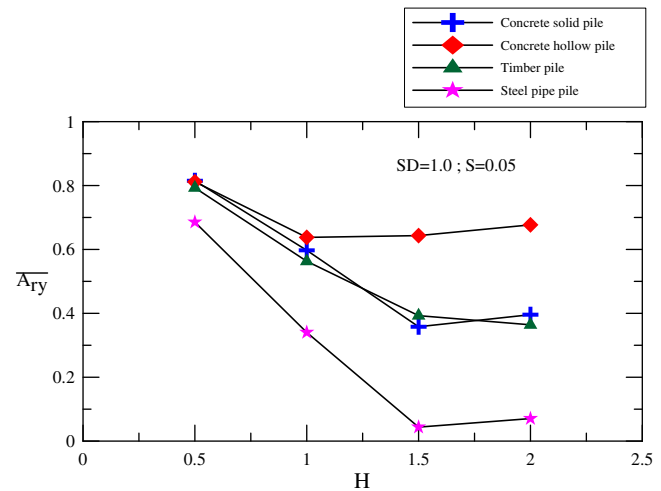

Fig. 15. Influence of the length parameter, H, on $\overline{A_{ry}}$ for the four types of piles (SD = 1.0, S = 0.05).
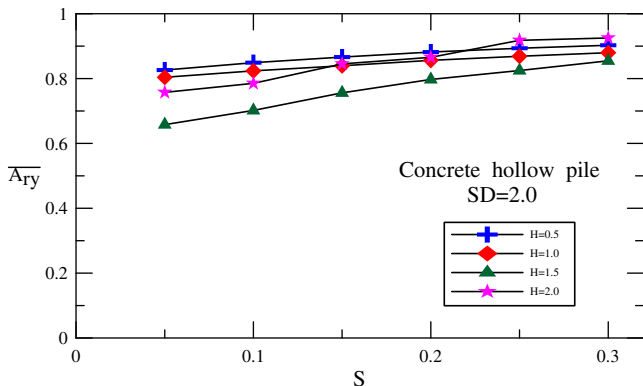

Fig. 13. Influence of net spacing parameter, S, on $\overline{A_{ry}}$-concrete hollow pile.
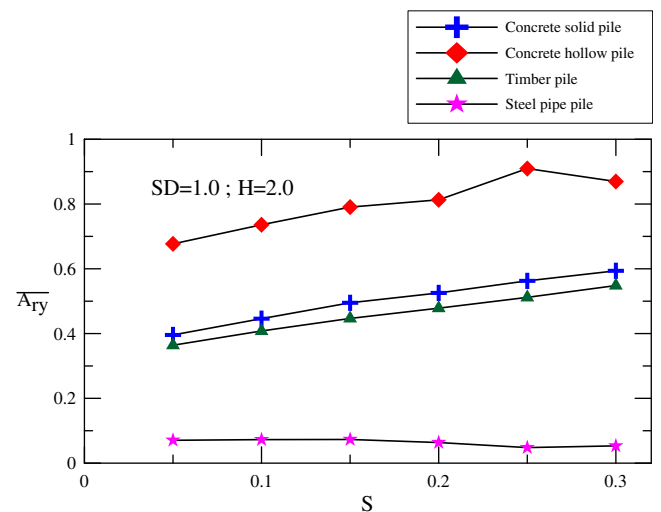

Fig. 16. Influence of the net spacing parameter, S, on $\overline{A_{ry}}$ for the four types of piles (H = 2.0, SD = 1.0).
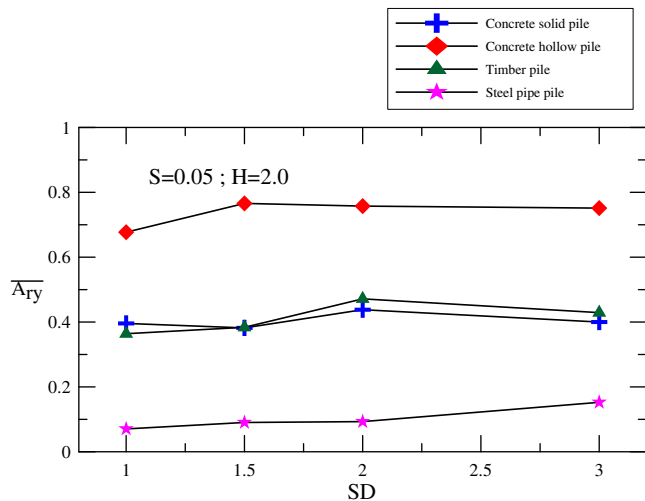
Fig. 17. Influence of the source distance parameter, SD, on $\overline{A_{ry}}$ for the four types of piles ($S = 0.05$, $H = 2.0$).

their shear moduli are close. The performance of concrete solid piles is better than that of concrete hollow piles, because the stiffness of concrete solid piles is larger than that of concrete hollow piles. This made the screening effectiveness of concrete hollow piles is the worst among the four types of barriers. The authors consider that the isolation effectiveness of pile barriers could depend on their shear modulus and stiffness.

To study the influence of vibration frequency on screening effectiveness for the four types of piles, we fixed the length of piles to 10 m, pile diameter to 1 m, source distance to 10 m, also assumed the net spacing as 0.5 m, and 5 vibration frequencies at 30 Hz, 40 Hz, 50 Hz, 60 Hz and 70 Hz. The results are shown in Fig. 18. For pipe pile barriers, the $\overline{A_{ry}}$ are around 0.1–0.15 for operational frequency of 30–70 Hz. It is still perform the best among the four
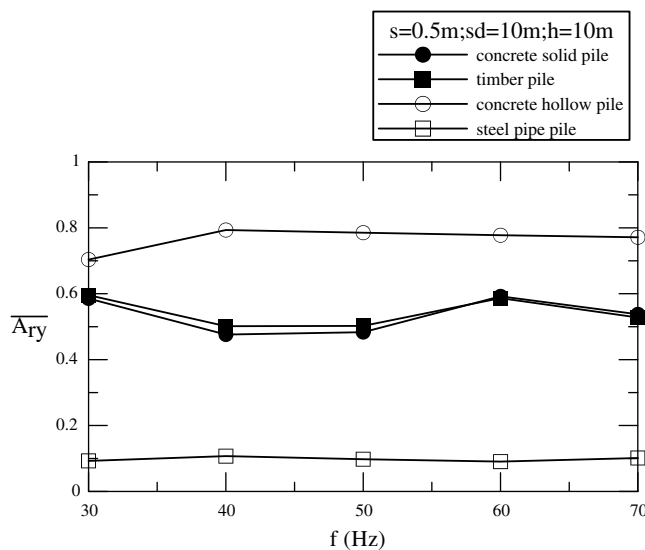
types of pile barriers. The $\overline{A_{ry}}$-curves of concrete solid piles and timber piles are again similar with $\overline{A_{ry}}$-curves ranging from 0.4 to 0.6. The concrete hollow piles are still relatively ineffective. It is also concluded that the screening effectiveness of pile barriers is insensitive to vibration frequency.

7. Conclusions

This research used 3-D frequency domain BEM to analyze screening effectiveness of pile barriers for rigid massless square foundation under harmonic vertical loading. Four types of circular piles were studied, including steel pipe piles, concrete hollow piles, concrete solid piles, and timber solid piles. The influence parameters discussed include dimension and layout of piles, source distance and vibration frequency. This study concludes the screening effectiveness using piles as vibration barriers as following:

1. The length of pile is the most important factor influencing the screening effectiveness. General, the longer the pile length is, the better the screening effectiveness would be. There are exception cases with steel pipe piles, however, these exception cases already have very good screening effectiveness ($\overline{A_{ry}} < 0.15$). The net spacing between piles and the source distance are less significant for screening effectiveness.
2. Using steel pipe pile for vibration screening is most effective among the four types of piles studied.
3. The screening effectiveness of timber pile and concrete solid pile is very similar. This phenomenon may be due to that the shear moduli of the timber pile and concrete solid pile are close.
4. Screening effective between structured hollow pile barriers and cylindrical cavity pile barrier could be very different.
5. Screening effectiveness of pile barriers is insensitive to vibration frequency.

Acknowledgements

References

[1] Barkan DD. Dynamics of bases and foundations Translated from Russian by Drashevska L and translation Tschebotarioff, GP. New York: McGraw-Hill; 1962. p. 434.
[2] McNeill RL, Margason BE, Babcock FM. The role of soil dynamics in the design of stable test pads. In: Proceedings of guidance and control conference, Minneapolis, Minnesota, 16–18 August, 1965. p. 366–75.
[3] Woods RD. Screening of surface waves in soil. J Soil Mech Foundation Eng (ASCE) 1968;94(SM4):951–79.

Fig. 18. Influence of vibration frequency on $\overline{A_{ry}}$ for the four types of piles ($s = 0.5$ m, sd = 10 m, h = 10 m).

[4] Woods RD, Barnett NE, Sagesser R. Holography, a new tool for soil dynamics. J Geotechn Eng (ASCE) 1974;100(11):1231–47.

[5] Liao S, Sangrey DA. Use of piles as isolation barriers. J Geotechn Eng (ASCE) 1978;104(9):1139–52.

[6] Haupt WA. Model test on screening of surface waves. In: Proceedings of the 10th int conf soil mech and found. Engineering, Stockholm, vol. 3, 1981. p. 215–22.

[7] Wass G. Linear Two-dimensional analysis of soil dynamics problem in semi-infinite layered media. PhD thesis, University of California, Berkeley, 1972.

[8] Aboudi J. Elastic waves in half-space with thin barrier. J Eng Mech (ASCE) 1973;99(1):69–83.

[9] Haupt WA. Surface waves in nonhomogeneous half-space. In: Prange B, editor. Dynamic methods in soil and rock mechanics. Rotterdam: Balkema; 1977. p. 335–67.

[10] Segol GP, Lee CY, Abel JE. Amplitude reduction of surface wave by trenches. J Eng Mech (ASCE) 1978;104(3):621–41.

[11] Fuyuki M, Matsumoto Y. Finite difference analysis of rayleigh wave scattering at a trench. Bull Seismol Soc Amer 1980;70:2051–69.

[12] May TW, Bolt BA. The effectiveness of trench in reducing seismic motion. Earthquake Eng Struct Dynam 1982;10:195–210.

[13] Avilles J, Sanchez-Sesma FJ. Piles as barriers for elastic waves. J Geotechn Eng (ASCE) 1983;109:1133–46.

[14] Emad K, Manolis GD. Shallow trenches and propagation of surface waves. J Eng Mech (ASCE) 1985;111(2):279–82.

[15] Beskos DE, Dasgupta G, Vardoulakis IG. Vibration isolation using open or filled trench. Part 1: 2-D homogeneous. Comput Mech 1986;1(1):43–63.

[16] Dasgupta B, Beskos DE, Vordouclakis IG. 3-D vibration isolation using open trenches. In: Innovative. Berlin: Springer-Verlag; 1986. p. 385–92.

[17] Dasgupta B, Beskos DE, Vordouclakis IG. Vibration isolation using open or filled trenches. Part 2: 3-D homogeneous soil. Comput Mech 1990;6:129–42.

[18] Avilles J, Sanchez-Sesma FJ. Foundation isolation from vibration using piles as barriers. J Eng Mech (ASCE) 1988;114:1854–70.

[19] Ahmad S, Al-Hussaini TM. Simplified design for open and in-filled trenches. J Geotechn Eng (ASCE) 1991;117(1):67–88.

[20] Klein R, Antes H, Houedec DL. Efficient 3D modelling of vibration isolation by open trenches. Comput Struct 1997;64:809–17.

[21] Kattis SE, Polyzos D, Beskos DE. Modelling of pile wave barriers by effective trenches and their screening effectiveness. Soil Dynam Earthquake Eng 1999;18:1–10.

[22] Kattis SE, Polyzos D, Beskos DE. Vibration isolation by a row of piles using a 3-D frequency domain BEM. Int J Numer Methods Eng 1999;46:713–28.

[23] Kupradze VD. Potential methods in the theory of elasticity. Israel Program for Scientific Translations, Jerusalem, 1965.

[24] Kitahara M, Nakagawa K. Boundary integral equation methods in three dimensional elastodynamics. In: Brebbia CA, Maier G, editors. Proceedings of the 7th international conference, Villa Olmo, Lake Como, Italy. Berlin, Heidelberg, New York: Springer (Boundary elements 7); 1985. p. 6.27–30.

[25] Beskos DE. Boundary element methods in mechanics. Computational methods in mechanics, vol. 3. Elsevier Science Publishers, BV; 1987.

[26] Zabreyko PP, Koshelev AI, Krasnoselskii MA, Mikhlin SG, Rakovshchik LS, Stetsenko VY. Integral Equations – A Reference Text. Leyden: Noordhoff International Publishing; 1975.

[27] Lysmer J. Foundation vibrations with soil damping. In: Proceedings of the 2nd ASCE conference on civil engineering and nuclear power, vol. II. Paper 10-4, Knoxville Tennessee, 1980. p. 1–18.

[28] Brebbia CA, Telles JCF, Wrobel LC. Boundary element techniques. Springer-Verlag; 1984.

[29] Becker EB, Carey GF, Oden JT. Finite elements – an introduction, vol. I. Prentice-Hall, Inc.; 1981.

[30] Wolfenden A, Hodge JQ. Dynamic shear modulus and damping in iron–copper and steel-based metal matrix composites. J Test Eval 2000;28(3):176–81.

[31] Vobolis J, Aleksiejunas M. Investigation of wood mechanical properties by the resonance vibration method. Mater Sci 2003;9(1):139–43.